lubricants

MDPI

Article

Analysis of Oil-Gas Two-Phase Flow Characteristics of Bearing Chamber Sealing System with Baffle Structure

Guozhe Ren [1,*], Rui Wang [1], Mingzhang Wang [2], Huan Zhao [1] and Wenfeng Xu [1]

[1] School of Aero-Engine, Shenyang Aerospace University, Shenyang 110000, China
[2] AECC Key Laboratory of Power Transmission for Aero Engine, AECC Shenyang Engine Research Institute, Shenyang 110000, China
* Correspondence: renguozhe7917@163.com; Tel.: +86-13390576961

Abstract

In order to explore the influence of baffle structure on the oil–gas two-phase flow and leakage characteristics of aero-engine bearing chamber sealing systems, based on the VOF two-phase flow model, this paper systematically carried out a transient numerical simulation of the bearing chamber sealing systems with conventional configurations and baffle configurations. The oil distribution, leakage and flow evolution of the two types of configurations under different baffle heights, sealing pressure differences and rotational speeds were compared and analyzed. The results show that the higher the height of the baffle, the more obvious the accumulation effect of the lubricating oil and the greater the leakage. The increase in sealing pressure difference helps to suppress leakage and reduce leakage fluctuation. The increase in rotational speed aggravates the centrifugal effect of the lubricating oil and makes the leakage increase significantly. This paper reveals the multi-parameter coupling mechanism of the baffle structure on the leakage control of the bearing chamber sealing system, and it provides a theoretical basis for the optimal design of the bearing chamber sealing structure of the aero-engine.

Keywords: bearing chamber; oil–gas two phase; leakage; baffle; VOF

1. Introduction

As the key space of engine spindle support, the bearing chamber is one of the core components of lubrication systems. Modern aero-engines generally use gas barrier technology to prevent the leakage of lubricating oil in the bearing chamber. Figure 1 shows a typical gas barrier sealing scheme [1]. When the aero-engine lubrication system is running, the lubricating oil enters the bearing chamber through the injection device to form a multiphase flow of oil and gas mixing.

In recent years, the research on oil–gas two-phase flow characteristics and sealing technology in bearing chambers has become an important topic in the field of engineering thermophysics and fluid mechanics. Many scholars have systematically explored the flow characteristics, heat transfer mechanisms and structural optimization in the bearing chamber, and they have achieved fruitful research results. Chen et al. [2–5] conducted in-depth research on the dynamic behavior of oil droplets in the bearing chamber, and they proposed a complete set of analysis methods for oil droplet deposition characteristics. This study reveals the internal mechanism of oil film formation and development by establishing an energy transfer model between oil droplets and air. The results show that the deposition process of oil droplets in the bearing chamber is affected by the combined

Check for updates

Received: 24 March 2026
Revised: 22 April 2026
Accepted: 25 April 2026
Published: 30 April 2026

Copyright: © 2026 by the authors. Licensee MDPI, Basel, Switzerland. This article is an open access article distributed under the terms and conditions of the Creative Commons Attribution (CC BY) license.

effects of centrifugal force, viscous force and surface tension, and the distribution of oil film thickness in different regions is significantly different. In the study of heat transfer characteristics, Li Kun et al. [6] used the parametric analysis method to systematically investigate the influence of bearing chamber structure parameters on internal flow and heat transfer. Li Wei [7] first applied a mixture multiphase flow model and VOF (Volume of Fluid) model to the flow analysis of bearing chambers, and they compared the applicability of the two models in different flow regions. It is found that mixture model has higher accuracy in predicting oil phase distribution, while the VOF model is more suitable for interface tracking. Ren and Hu [8,9] deeply analyzed the influence mechanism of rotational speed on the distribution of lubricating oil through systematic numerical simulation and experimental research. The results show that under low speed conditions (usually less than 3000 r/min), the gravity effect dominates, and the oil mainly accumulates on the rotation direction side of the oil's return hole. When the speed is increased to more than 5000 r/min, the centrifugal force effect is significantly enhanced, and the distribution of the oil film on the chamber wall tends to be uniform.

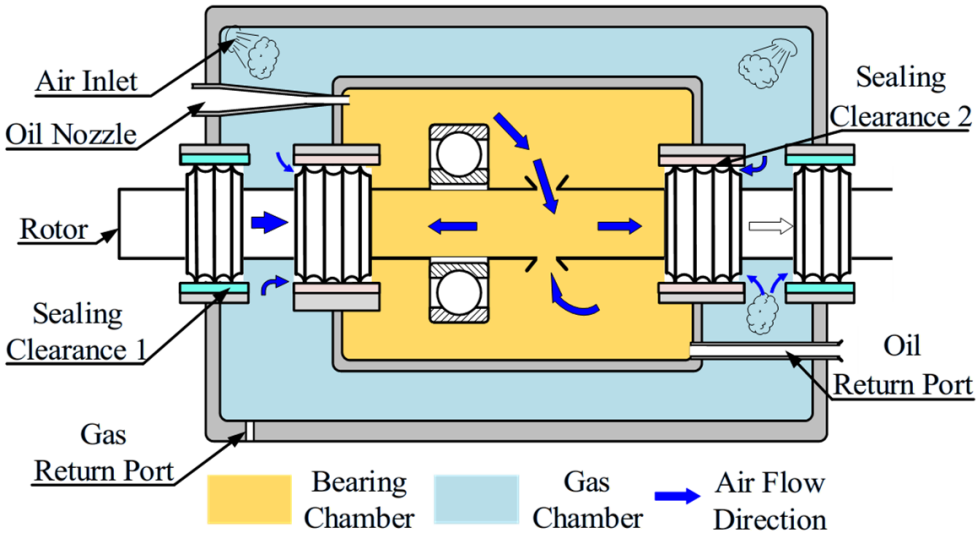


Figure 1. Aero-engine bearing chamber air-entrained seal schematic diagram.

In order to improve the oil return performance of the bearing chamber, Ren [10] proposed three innovative oil return structure design schemes. The first one adopts the design of a spiral guide groove, which guides the oil flow to the oil return port. The second one optimizes the ventilation structure and uses the air flow to assist the oil return. The third one combines the advantages of the previous two schemes and adopts the composite structure. Through comparative analysis, it is found that the composite structure can maintain high oil return efficiency in a wide speed range, especially under high speed conditions. Cao et al. [11] developed a numerical simulation technique based on the CLSVOF (Couple Level Set and Volume of Fluid) method for the common double-pivot counter-rotating bearing chamber in aero-engines. The study reveals the particularity of the oil phase distribution under the counter-rotating condition. Due to the reverse rotation of the two rotors, a complex vortex structure is formed in the middle region, which has an important influence on the heat transfer characteristics. In the follow-up study, the team further investigated the influence of the sealing air flow on the thermal environment of the bearing chamber, and they found that an appropriate increase in the sealing air flow can effectively reduce the temperature of the bearing chamber outer wall, but too large air flow will lead to excessive purging of the lubricating oil, which will affect the lubrication effect [12]. Gu [13] studied the oil return efficiency under different working conditions by

combining experiment and simulation. The data show that when the speed is increased from 2000 r/min to 8000 r/min, the oil retention can be reduced by about 40%. Caixia Li [14] focused on the special flow characteristics of a single-outlet bearing chamber. The effects of rotational speed and fuel delivery on the secondary flow pattern were analyzed by three-dimensional numerical simulation. It is found that under steady-state conditions, increasing the rotational speed and fuel delivery can improve the uniformity of oil film thickness, but when the rotational speed exceeds a certain critical value, the oil film thickness will decrease instead. This nonlinear relationship indicates that the operating parameters need to be optimized according to the specific operating conditions. Li et al. [15] used the multi-physical field coupling simulation method to pay attention to the relationship between the volume fraction of the oil phase and the local heat transfer coefficient, and they found that the heat transfer efficiency of the low concentration oil phase region was low. Aiming at the special requirements of high-speed angular contact ball bearings, Wang et al. [16] studied the influence of oil and gas outlet position on lubrication performance by using a VOF model combined with the MRF (Multiple Reference Frame) method. The numerical simulation results show that the reasonable design of the outlet position can effectively control the volume fraction of the oil phase in the chamber and control the temperature rise of the key parts within a safe range. Yang [17,18] improved the structure of the traditional oil return groove. The effects of groove depth, groove width and other parameters on the oil return performance were systematically studied by unsteady numerical simulation. It is found that increasing the groove depth appropriately can improve the oil capture efficiency, but too deep will lead to an increase in flow resistance. The optimized oil return groove structure can increase the oil return ratio by more than 25%, and the wall heat transfer coefficient is increased by about 15%. Fang [19] focused on the coking problem caused by lubricating oil overheating. The flow characteristics of the lubricating oil under different working conditions were analyzed by CFD simulation. It was found that increasing the rotational speed can enhance the wall velocity and improve the heat transfer conditions. Aiming at the problem of return pipe blockage, the performance of return pipes with circular, square and triangular cross-sections was studied and compared. Finally, a new composite cross-section design was proposed, which achieved a good balance between anti-blocking performance and flow resistance. Based on the traditional one-way coupling model, Lv et al. [20] proposed a two-way coupling model considering the interaction force between phases. Through comparative analysis, it is found that the new model can predict the turbulence characteristics in the chamber more accurately, especially under high speed conditions, and the prediction accuracy of the air velocity field is significantly improved. The study of ZhaoChen Hu [21] revealed the influence of oil supply parameters on the distribution of lubricating oil, and the VOF method was used to simulate the flow characteristics under different combinations of oil supply and rotational speed. The results show that increasing the rotational speed will cause the lubricating oil to accumulate to the upper part of the chamber and prolong its stay time in the chamber, while increasing the oil supply will cause more lubricating oil to accumulate at the bottom, but the overall stay time will be shortened.

Glahn et al. [22–24] carried out experimental research on the formation mechanism of oil droplets in the bearing chamber by designing a variety of lubrication injection structures, and they revealed the variation in oil droplet size and velocity under different injection modes (rotating disk, axial channel, radial hole). The results show that there is a significant correlation between the diameter of oil droplets and the Weber number. The particle size decreases with the increase in rotational speed in a specific range of rotational speed, but it tends to be stable after reaching the critical speed. In addition, the average size of oil droplets is positively correlated with the thickness of the oil film. Lee's team [25]

constructed an experimental system based on the aero-engine bearing chamber, and they used particle image velocimetry to observe the airflow characteristics. It was confirmed that the rotational speed and the chamber structure would significantly change the flow field morphology. The numerical simulation shows that the RMS turbulence model has high calculation accuracy. Gores et al. [26] found that there was vortex flow in the chamber by using a laser Doppler velocimeter, and they quantified the influence of rotational speed and air intake on the vortex structure. Aidarinis et al. [27] innovatively established a numerical model of the bearing equivalent to the porous medium, and they verified the reliability of simulation combined with LDA experimental data. Farrall et al. [28] established a wall film dynamics model covering the movement of oil droplets and the process of collision deposition, which provides a theoretical basis for related research.

By simplifying the assumption of axial oil film motion, Chew [29] constructed a one-dimensional oil–gas coupling model considering aerodynamic energy exchange, and they revealed the quantitative relationship between oil film thickness and flow velocity. Based on the depth-average theory, Farrall et al. [30] established a steady-state laminar oil film model considering air drag effect and gravity effect, and they realized the coupling solution of oil film thickness and airflow velocity. In order to improve the limitations of the traditional VOF method, Hashmi et al. [31] proposed an interface capture technique by modifying the turbulent source term, which effectively improved the simulation accuracy of stratified flow. Peduto et al. [32] applied this improved method to study the oil film fluctuation characteristics in the oil return area, and they successfully captured the dynamic characteristics of the gas–liquid interface by coupling the VOF and k-ε models. Crouchez et al. [33] used a numerical strategy combining adaptive mesh and the VOF to ensure the calculation accuracy while significantly reducing the amount of mesh, accurately reconstructing the oil–gas interface morphology and obtaining the oil distribution cloud map under key working conditions. Adeniyi et al. [34] revealed the time-varying law of wall heat transfer coefficient and the evolution process of oil flow under the special oil return structure by unsteady simulation. Based on the particle method simulation, Wieth et al. [35] found that the oil film distribution on the wall is more uniform at high speed (15,000 r/min), and the oil phase diffuses significantly to the central region of the chamber. Li et al. [36] systematically studied the two-phase flow mechanism of the bearing chamber sealing system, and they confirmed that the increase in the rotational speed will aggravate the oil leakage, while the increase in the pressure difference has an inhibitory effect. In particular, it is found that the reverse thread structure can reduce the leakage by about 40%, which provides a new idea for sealing optimization.

In summary, the existing research has carried out extensive and in-depth discussions on the oil–air two-phase flow characteristics, heat transfer mechanism and oil return structure optimization in the bearing chamber, especially regarding the aspects of oil droplet movement behavior, oil film distribution law, oil return efficiency improvement and the applicability of numerical simulation methods. However, the current research mostly focuses on the conventional bearing chamber structure, and there is still a lack of systematic research on the influence mechanism of active control structures such as baffles on the transient leakage characteristics, the oil and gas distribution patterns, and the sealing performance of the bearing chamber sealing system. In particular, under the coupling effect of different baffle heights, sealing pressure differences and rotational speeds, the transient response law and leakage control mechanism of oil–gas two-phase flow in the sealing system are not clear. Therefore, based on the VOF two phase flow model, this paper systematically studies the influence of baffle structure on the oil–gas two-phase flow and leakage characteristics of bearing chamber sealing systems. By comparing and analyzing the transient flow characteristics, oil–gas distribution laws and leakage dynamic behaviors

of conventional configurations and baffle configurations, the sealing mechanism under the coupling of multi-parameters such as baffle height, sealing pressure difference and rotating speed is revealed, which can provide a theoretical basis and technical reference for the design optimization and performance improvement of the bearing chamber sealing structures of aero-engines.

2. Numerical Simulation Method of Bearing Chamber Sealing System Characteristics

2.1. Geometric Model of Bearing Chamber Sealing System

Figure 2 shows the overall structural layout of the conventional bearing chamber sealing system. The system is composed of three key parts, which are the sealing chamber, graphite sealing gap and bearing chamber in turn along the axial direction. From left to right, it can be seen that the sealing chamber is located on the left side with an axial width of 25 mm. There are eight inlets evenly distributed in the circumferential direction of the sealing chamber for the introduction of sealing gas. The length of each inlet is 15 mm, and the diameter is 6 mm. The middle part is a graphite sealing gap, which is simplified as an annular gap in the analysis. The design of the bearing chamber on the right side is more complicated with an axial width of 30 mm. It has eight lubricating oil injection holes evenly arranged along the circumference and the same size as the air inlet. A ventilation structure is also arranged at the top of the chamber. At the same time, a special oil return channel is set at the bottom. The vent and oil return port are both cylindrical structures with a length of 15 mm and a diameter of 10 mm.

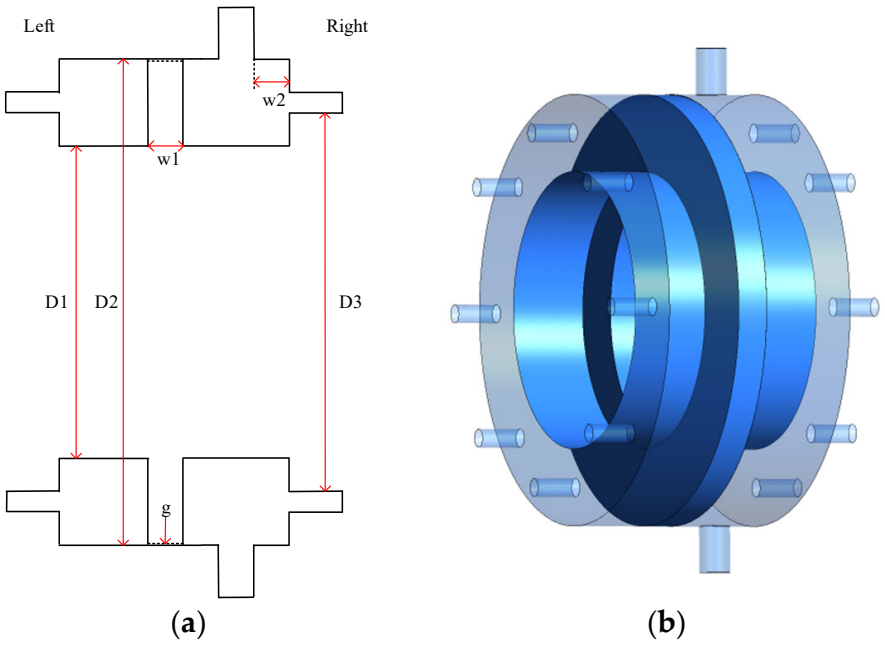


Figure 2. The bearing chamber sealing system of conventional configuration: (**a**) two-dimensional schematic; (**b**) geometric model.

In order to analyze the influence of the baffle structure on the bearing chamber sealing system, the baffle structure is added to the conventional bearing chamber sealing system. Figure 3 shows the overall structural layout of the bearing chamber sealing system with the baffle configuration. The left side of the baffle is 2 mm from the graphite ring, the baffle width t = 3 mm, and the height of the baffle is set to 5 mm, 10 mm and 15 mm, respectively. The remaining specific structural parameters are shown in Table 1.

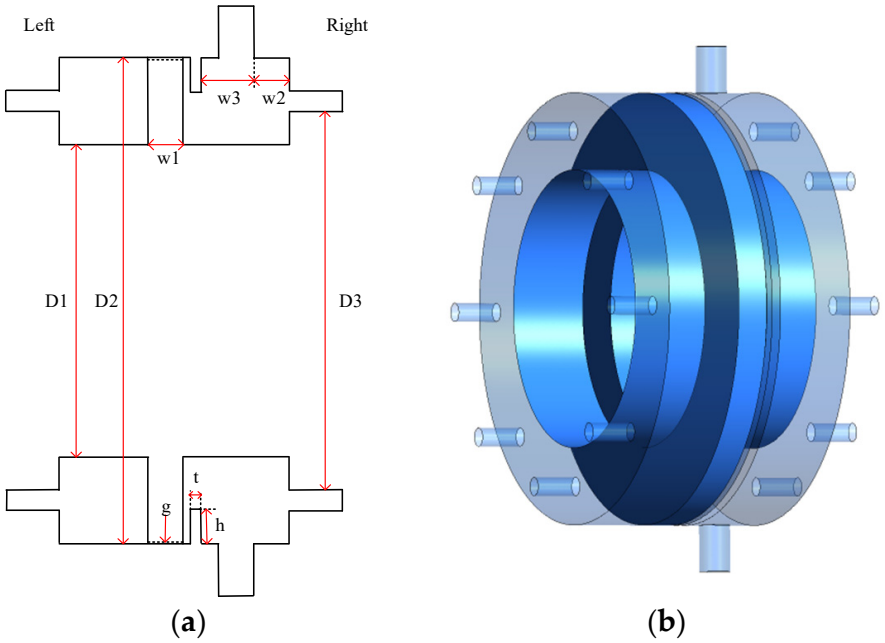


Figure 3. The bearing chamber sealing system of baffle configuration: (**a**) two-dimensional schematic; (**b**) geometric model.

Table 1. Geometric model structure parameters.

Parameter	Value
D1/mm	90
D2/mm	140
D3/mm	54.5
w1/mm	10
w2/mm	10
w3/mm	10
g/mm	0.05
t/mm	3
h/mm	5, 10, 15

2.2. Meshing and Boundary Conditions

In the process of meshing, ANSYS 2022 R1 Meshing software is used to refine the solution model. Different grid strategies are adopted according to the structural characteristics of different regions. For the graphite seal gap region, a structured grid division method is used to ensure that the flow parameters in the region can be accurately analyzed, and the number of grid layers is 10. In the thin layer of the sealing chamber and the bearing chamber connected to the graphite seal gap, the structured grid is also used to prevent the grid quality from being too low. The other parts use unstructured grids, as shown in Figure 4. The method of dividing the processing grid into different regions can effectively avoid the numerical error caused by poor grid quality, which lays a good numerical calculation foundation for subsequent flow field analysis.

The air inlet is set as the entrance of the opening, the intake temperature is 25 °C, and the intake pressure is set to 0.1075 MPa, 0.11 MPa and 0.115 MPa according to different working conditions. The oil inlet is set as the entrance of the inlet, the mass flow rate is 0.1 kg/s, and the oil inlet temperature is 60 °C. Both the air vent and the oil return port are static pressure outlets. The rotate speed of the rotational surface is 5000 r/min, 10,000 r/min and 15,000 r/min according to different working conditions. The specific boundary conditions are shown in Figure 5 and Table 2.

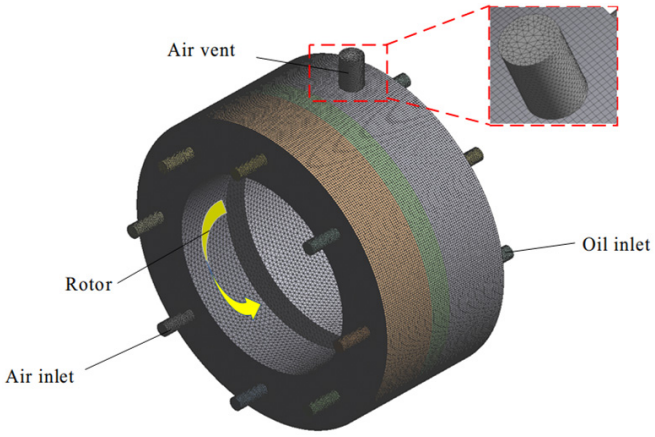


Figure 4. Grid division of bearing chamber sealing system.

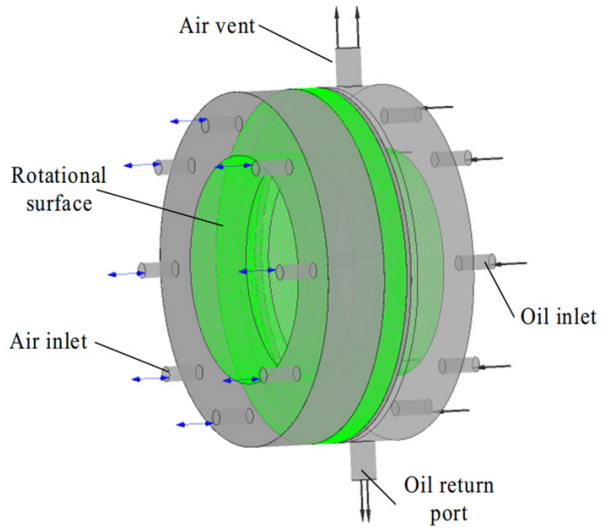


Figure 5. Boundary condition setting.

Table 2. Boundary condition parameter setting.

Parameter	Value
Air inlet pressure/MPa	0.1075, 0.11, 0.115
Oil inlet flow/(kg/s)	0.1
Air vent pressure/MPa	0.1
Oil return port pressure/MPa	0.1
Rotate speed/(r/min)	5000, 10,000, 15,000

2.3. Accuracy Verification

In order to ensure the reliability of the numerical simulation results, an experimental device for obtaining the oil and gas leakage characteristics of the micro-gap of the bearing chamber was designed and built. As shown in Figure 6, the system introduces the pressurized air into the core section of the experimental device through the gas storage tank, and the air enters the gas chamber from the bottom. A small gap is formed between the sealing gap control disc and the wall surface, and the gap size is changed by changing the radius of the disc. The oil chamber is located in the upper part, the lubricating oil is filled from the upper part, and the stable oil chamber pressure is maintained through the opening. Figure 6 shows (a) the principle of the experimental device, (b) the physical map of the experimental device, and (c) the two-dimensional profile diagram of the core section of the experimental device.

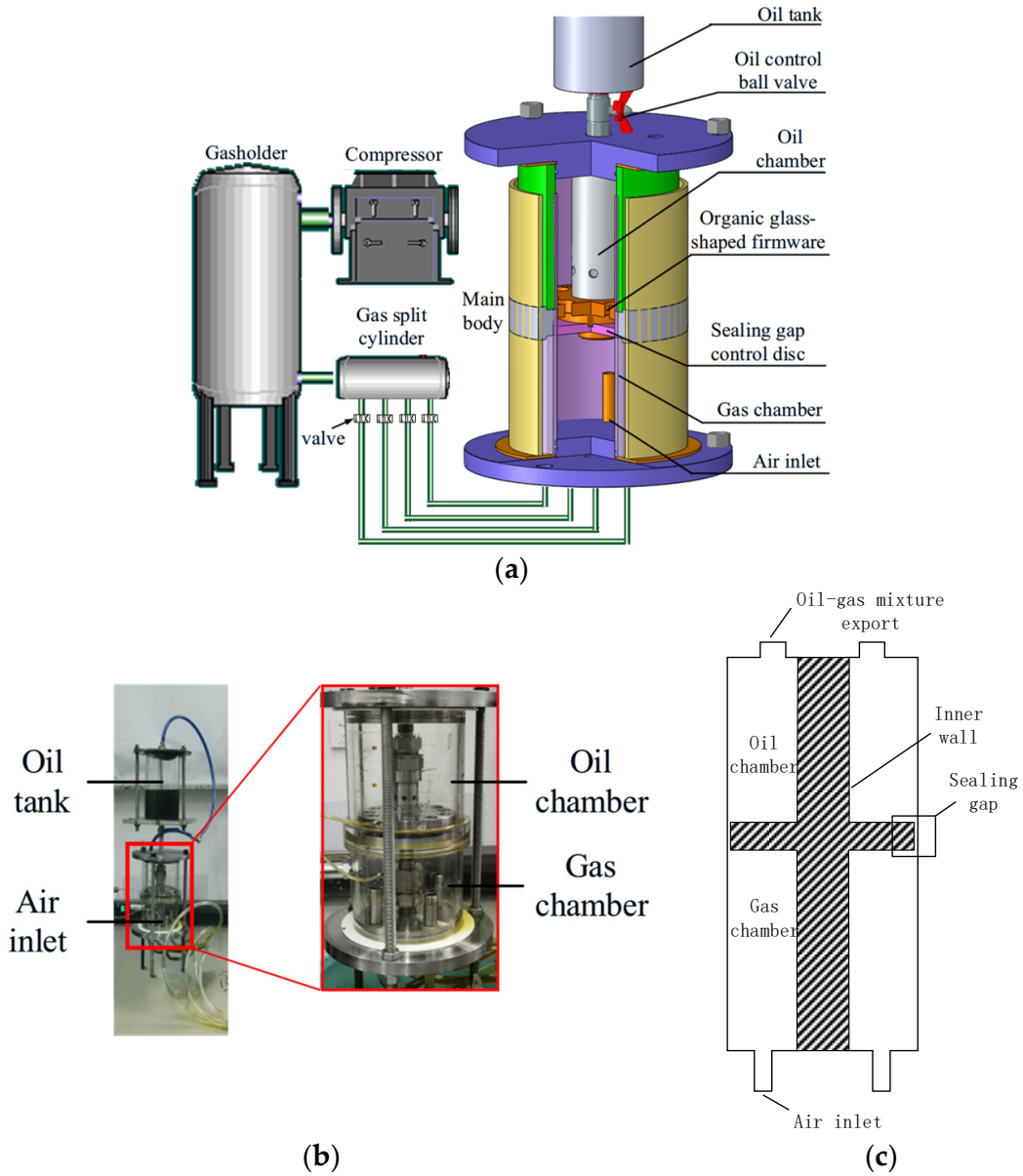


Figure 6. Experimental device: (**a**) principle schematic diagram; (**b**) object picture; (**c**) two-dimensional schematic.

In the experiment, 4106 aviation lubricating oil was selected as the research object. Considering the almost colorless and transparent characteristics of the lubricating oil, in order to facilitate experimental observation, dark stain was added to the lubricating oil to enhance the visualization effect. In the experiment, firstly, the compressed air is injected into the gas chamber, and the initial pressure barrier is established to ensure that the lubricating oil does not penetrate into the gas chamber area. After the air pressure is stabilized, the oil is injected into the oil chamber to a predetermined liquid level height. At this time, the system reaches equilibrium, and the oil neither enters the sealing gap nor flows to the gas chamber. Subsequently, the suction pressure is gradually reduced by a precise pressure regulating device. When the pressure drops to a certain critical value, it can be observed that the oil begins to migrate slowly to the air chamber. Through the high-speed camera system, the movement process of the oil–gas interface is monitored in real time. When the interface is close to the outlet of the gas chamber side of the sealing gap, the air pressure is immediately and stably controlled to prevent the oil from continuing to leak. When the system reaches a new equilibrium state, a high-precision differential pressure transmitter is

used to measure the pressure difference (ΔP) between the top of the gas chamber and the bottom of the oil chamber. This measurement process needs to be repeated many times to ensure the reliability of the data.

The numerical simulation of the oil and gas leakage characteristics of the micro-gap of the bearing chamber is carried out. Figure 7 shows the geometric model of the numerical simulation of the experimental device. Compared with the experimental device, the geometric model is simplified and the key structure is retained, such as ignoring the organic glass solid parts that prevent the deformation of the chamber wall. Figure 8 shows the meshing of the numerical simulation of the experimental device. Due to the small width of the sealing gap, mesh refinement is applied to this region. After refinement, the number of axial nodes of the sealing gap is 32, and the number of circumferential nodes is 50. The width of the sealing gap is 0.05 mm, the number of radial grid nodes of the model is 8, and the number of grids is 3.624 million. The boundary conditions of the numerical simulation of the experimental device are set as shown in Table 3.

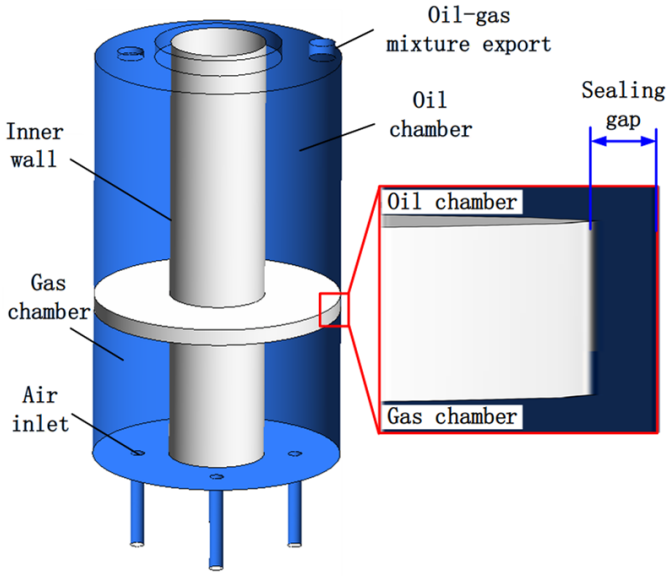


Figure 7. Geometric model of numerical simulation of experimental device.

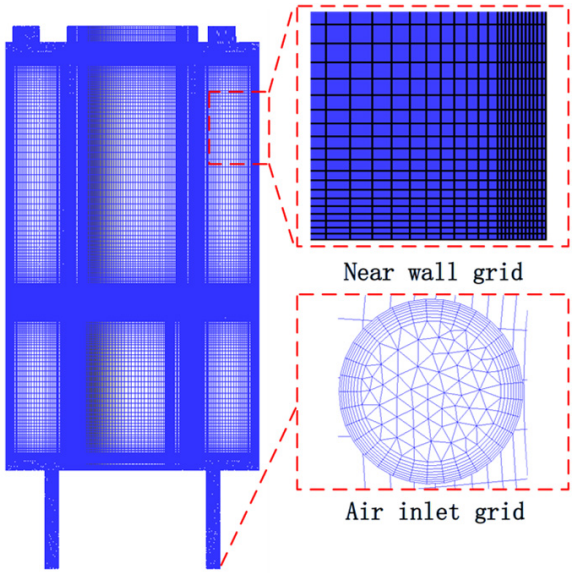


Figure 8. Meshing of numerical simulation of experimental device.

Table 3. Boundary conditions of the numerical simulation of the experimental device.

Parameter	Value
Air inlet total pressure/Pa	200~2000
Export pressure/Pa	0
Reference pressure/atm	1
Gravitational acceleration/m/s^2	9.8
Lubricating oil height/mm	30~120
Lubricating oil temperature/°C	25
Two-phase flow model	Mixture
Turbulent model	SST

Figure 9 shows the comparison between the numerical results and the experimental results of the critical sealing pressure at different lubricating oil heights. The average error between the two is 14.5%. At the same time, it can be seen that the numerical simulation is consistent with the change law of the critical sealing pressure obtained by the experiment. The numerical and experimental errors are mainly caused by the following reasons: the physical parameters of the lubricating oil used in the experiment cannot be completely consistent with the lubricating oil parameters in the numerical solution, resulting in errors between the experiment and the numerical simulation value. Compared with the experimental device, the numerical model ignores the organic glass solid parts, and the organic glass solid parts occupies a small part of the oil chamber volume. This results in a slight difference in the quality of the lubricating oil when the lubricating oil height is fixed in the numerical simulation and experiment, which leads to numerical and experimental errors. There is a machining error in the sealing gap control disc used in the experiment.

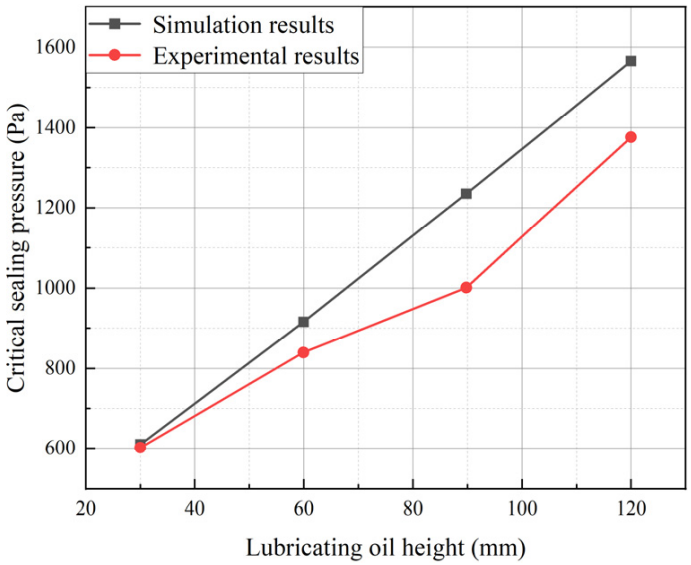


Figure 9. Comparison of experimental and numerical results of critical sealing pressure at different lubricating oil heights.

2.4. Grid Independence Verification

In order to reduce the influence of the number of grids on the calculation results, the lubricating oil leakage of the numerical model of the bearing cavity sealing system with different number of grids is solved. In the numerical solution, when the relative error of the lubricating oil leakage caused by the number of grids does not exceed 0.5%, it can be considered that the number of grids has little effect on the calculation results. Figure 10 shows the change in lubricating oil leakage with the number of grids under different baffle

heights. After grid independence verification, when the baffle height is 0 mm, 5 mm, 10 mm and 15 mm, the number of grids is 4.114 million, 3.762 million, 3.436 million and 3.136 million, respectively.

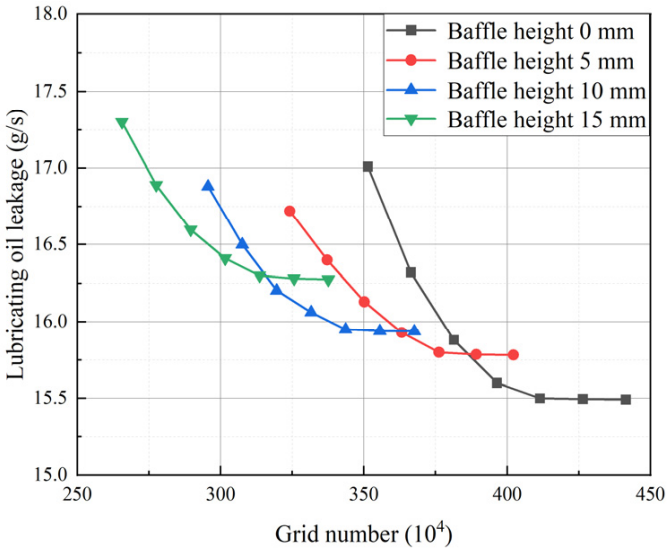


Figure 10. The change in lubricating oil leakage with the number of grids.

3. Analysis of Oil–Gas Two-Phase Flow Field in Bearing Chamber Sealing System

3.1. The Influence of Baffle Structure on the Transient Characteristics of the Bearing Chamber Sealing System

Figure 11 shows the change in oil volume fraction with time of bearing chamber sealing systems with conventional configurations and baffle configurations. The working conditions are a sealing pressure difference of 10 kPa, rotational speed of 15,000 r/min and baffle height of 10 mm. It can be seen from Figure 11 that the change in oil volume fraction of the bearing chamber sealing systems with a conventional configuration and a baffle configuration shows a similar trend, but it is still slightly different. The volume fraction of lubricating oil in the sealing chamber of the two configurations increases with time, showing a linear function relationship, indicating that leakage has occurred, but the volume fraction of lubricating oil after adding the baffle increases more—that is, the leakage rate of lubricating oil is greater. In order to facilitate the calculation, it is assumed that the lower part of the bearing chamber is filled with lubricating oil at the initial moment. As the simulation begins, the lubricating oil will flood into the sealing gap in large quantities, so the volume fraction of lubricating oil at the sealing gap will increase sharply. After that, it shows the characteristics of fluctuation and is stably maintained within a certain range. This is because the high-pressure gas in the sealing chamber flows to the bearing chamber through the sealing gap, which is against the lubricating oil and plays a sealing role. The volume fraction of lubricating oil at the sealing gap of the conventional configuration fluctuates in the range of 0.3~0.4, and the peak value is close to 0.45. The oil volume fraction of the bearing chamber seal system with baffle configuration fluctuates in the range of 0.55~0.8, which is more volatile than that of the conventional configuration, but the fluctuation frequency is lower. The volume fraction of lubricating oil in the bearing chamber increases slowly with time. The volume fraction of lubricating oil in the bearing chamber with the baffle configuration is higher than that in the conventional configuration, but the increase in the volume fraction of lubricating oil in the bearing chamber with the baffle configuration is more stable, similar to a straight line, while that in the conventional configuration is tortuous.

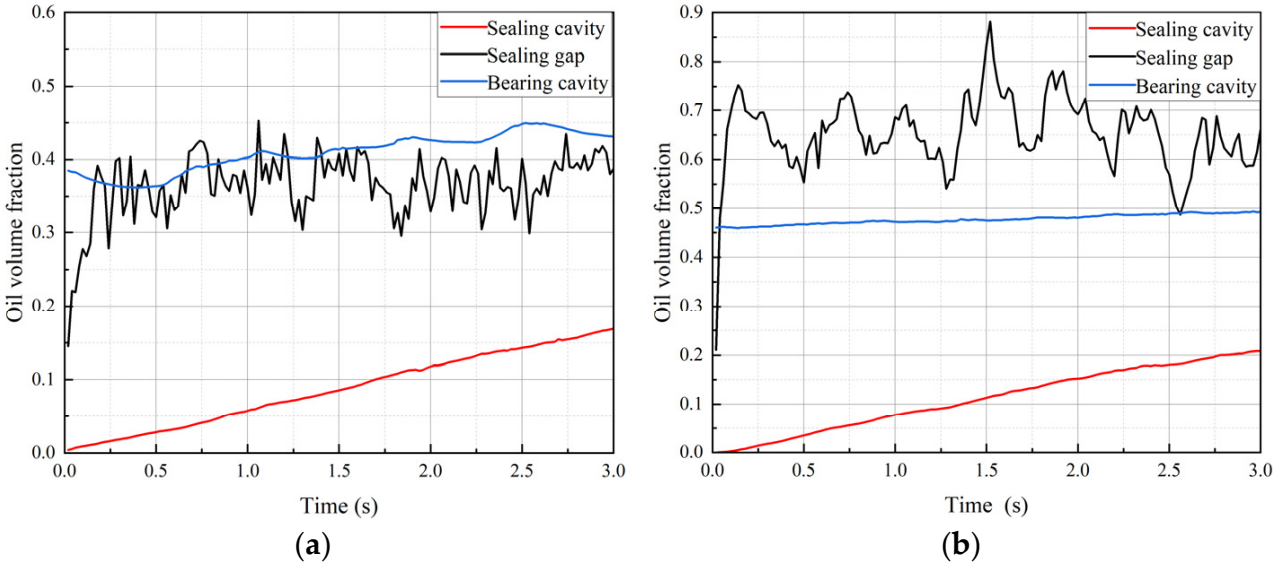


Figure 11. The change in oil volume fraction with time in different configurations (ΔP = 10 kPa, n = 15,000 r/min): (**a**) conventional configuration; (**b**) baffle configuration.

3.2. The Influence of the Baffle Structure on the Oil–Gas Two-Phase Distribution of the Bearing Chamber Sealing System

Figure 12 shows the oil volume fraction cloud diagram in the circumferential bearing chamber sealing systems with conventional configurations and baffle configurations. The working condition is a sealing pressure difference of 10 kPa, rotational speed of 15,000 r/min, and baffle height of 10 mm. It can be seen that the distribution of lubricating oil in the bearing chamber changes after adding the baffle. With the increase in time, the volume of lubricating oil in the sealing chamber increases continuously due to leakage, and the configuration with baffles increases slightly faster than the conventional configuration. For the conventional configuration, the lubricating oil in the bearing chamber presents a triangular distribution state, and it tends to be stable as the simulation progresses. This is due to the shear friction generated by the high-speed rotation of the rotating shaft, which makes the lubricating oil in the bearing chamber rotate and be centrifugally distributed on the inner wall of the bearing chamber. Because the sealing gas enters the bearing chamber axially through the sealing gap, the lubricating oil will be blown in a triangular distribution. After the baffle is added, the sealing gas no longer enters the bearing chamber axially but rather flows radially into the bearing chamber from the graphite ring wall and the baffle wall, and it blows first to the rotating shaft. Therefore, with the increase in time, the lubricating oil in the bearing chamber with baffles presents a complex and uncertain distribution state, and the sealing gas flowing along the radial direction makes the turbulence in the bearing chamber increase greatly.

Figure 13 shows the contour map of the oil volume fraction of 0.8 for the bearing chamber sealing systems with different configurations. The working condition is a sealing pressure difference of 10 kPa, rotation speed of 15,000 r/min, and baffle height of 10 mm. It can be seen that similar to the analysis in the previous section, the distribution of lubricating oil in the bearing chamber is changed after adding the baffle. In the conventional bearing chamber sealing system, the lubricating oil in the bearing chamber leaks to the sealing chamber through the sealing gap, and the lubricating oil is distributed on the inner wall of the whole system by centrifugal action. The volume of lubricating oil in the sealing chamber and sealing gap in the conventional bearing chamber sealing system is less than that in the bearing chamber sealing system with baffles, which is consistent with Figure 11. Due to the small disturbance of the sealing gas blowing into the bearing chamber along the

axial direction from the sealing gap, the lubricating oil of the conventional sealing system is evenly distributed on the inner wall surface, which is close to the 'laminar flow state'. For the configuration with baffles, the oil in the bearing chamber is subject to more complex and severe airflow shear force and is close to the 'turbulent state', showing a disturbed distribution. Compared with the conventional configuration, the oil movement of the baffle configuration is more intense, so the oil distribution is no longer close to the inner wall surface, and it can move to the small radius or the rotating shaft, which is more conducive to the lubrication and heat dissipation of the bearing inner ring, but it will also increase the leakage of the oil.

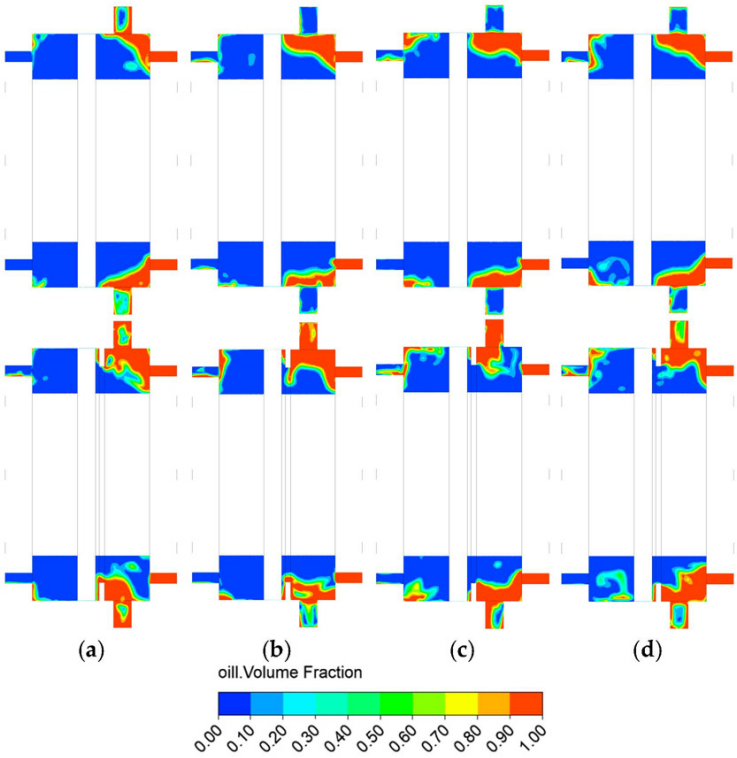


Figure 12. Section cloud diagrams of bearing chamber sealing system with conventional configuration and baffle configuration (ΔP = 10 kPa, n = 15,000 r/min): (**a**) t = 0.5 s; (**b**) t = 1 s; (**c**) t = 2 s; (**d**) t = 3 s.

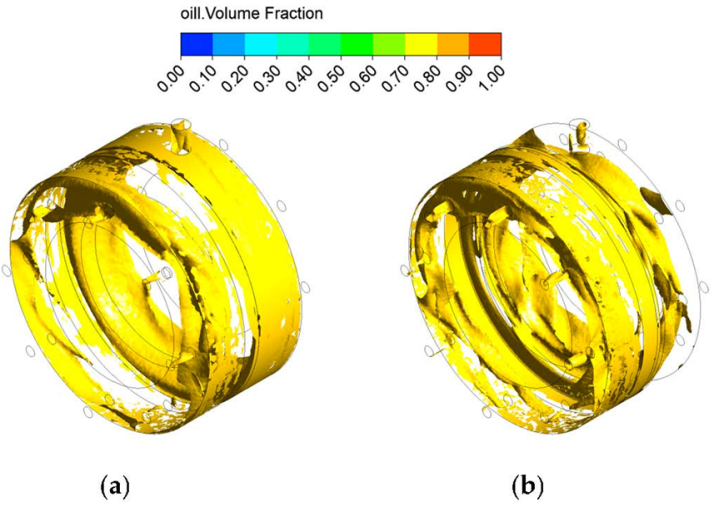


Figure 13. Isosurface diagrams of the bearing chamber sealing system with conventional configuration and baffle configuration when the oil volume fraction is 0.8 (ΔP = 10 kPa, n = 15,000 r/min, t = 3 s): (**a**) conventional configuration; (**b**) baffle configuration.

Figure 14 shows the contour map of the oil volume fraction of 0.2 for the bearing chamber sealing systems with different configurations. The working condition is a sealing pressure difference of 10 kPa, rotation speed of 15,000 r/min, and baffle height of 10 mm. It can be seen from the figure that the distribution state of the lubricating oil changes after the baffle is added, the fluctuation degree of the lubricating oil increases, and the movement range of the lubricating oil is closer to the rotation axis. It is worth noting that the area with a high proportion of oil volume in the conventional configuration is mostly distributed on the outside of the oil return hole, and the area with a low proportion is mostly distributed on the inside. Moreover, because the oil in the conventional configuration is close to the inner wall of the bearing chamber, the way of oil entering the oil return hole and the air vent is mostly 'scraped in'. The entry mode with the baffle configuration is mostly 'inflow'.

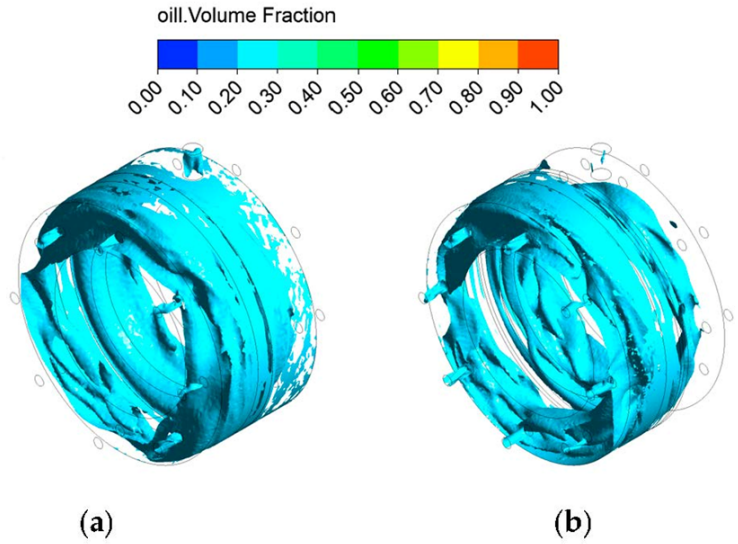


Figure 14. Isosurface diagrams of the bearing chamber sealing system with conventional configuration and baffle configuration when the oil volume fraction is 0.2 (ΔP = 10 kPa, n = 15,000 r/min, t = 3 s): (**a**) conventional configuration; (**b**) baffle configuration.

3.3. Influence of Baffle Structure on Leakage Characteristics of Bearing Chamber Sealing System

Figure 15 shows the variation in oil leakage with time in the conventional configuration and baffle configuration. The working condition is a sealing pressure difference is 10 kPa, rotation speed is 15,000 r/min, and baffle height is 10 mm. It can be seen that the oil leakage of the baffle configuration is slightly larger, which is consistent with the results of the sealing chamber in Figure 11. The oil leakage of the conventional configuration fluctuates in the range of 0~20 g/s for most of the time, and the peak value reaches 40 g/s. Before 1.5 s, the oil leakage of the baffle configuration is obviously larger than that of the conventional configuration. This is because the lower half of the bearing chamber is filled with lubricating oil at the initial time of simulation. The accumulation of lubricating oil between the baffle structure and the graphite ring is not easy to discharge, resulting in a larger oil leakage.

3.4. Summary of This Section

In this section, the flow field and leakage characteristics of the bearing chamber sealing systems with conventional configurations and with baffle configurations are compared and analyzed. The influence of baffle structure on the transient characteristics, oil–gas two-phase distribution and leakage characteristics of the sealing system is considered. The following conclusions are drawn:

(1) After adding the baffle, the volume fraction of the lubricating oil in the sealing chamber increases, the growth rate is 1.28 times that of the conventional configuration, and the volume fraction of the lubricating oil in the bearing chamber increases but the fluctuation is smaller.

(2) After adding the baffle, the distribution state of the lubricating oil in the bearing chamber changes. Due to the change in the entry direction of the sealing gas, the turbulence degree of the lubricating oil in the bearing chamber increases and the movement is more intense.

(3) The oil leakage of the bearing chamber sealing system with the baffle configuration is larger; this is due to the accumulation of lubricating oil between the baffle and the graphite ring.

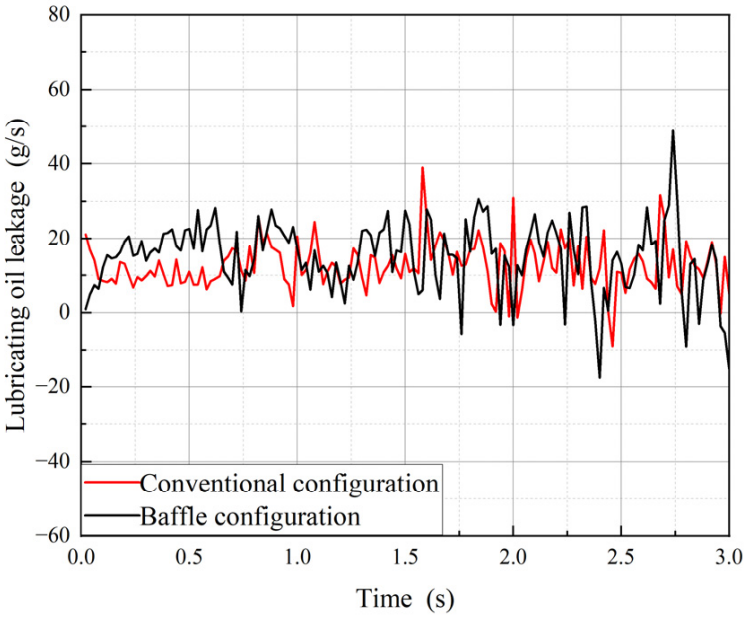


Figure 15. Variation in oil leakage with time for different configurations (ΔP = 10 kPa, n = 15,000 r/min).

4. Characteristic Analysis of Bearing Chamber Sealing System with Baffle Configuration

4.1. The Influence of Baffle Height on the Bearing Chamber Sealing System with Baffle

4.1.1. The Sealing Pressure Difference Is 7.5 kPa and the Rotational Speed Is 15,000 r/min

Figure 16 shows the change in oil leakage with different baffle heights under the condition of a sealing pressure difference of 7.5 kPa and rotational speed of 15,000 r/min. It can be seen that with the increase in baffle height, the leakage of lubricating oil also increases, and the degree of fluctuation increases. The oil leakage of the structure with a baffle height of 15 mm is significantly greater than that with the baffle height of 10 mm and 5 mm, but it is basically within 40 g/s, and the peak value can reach more than 60 g/s. In order to facilitate the calculation, it is assumed that the lower part of the bearing chamber is filled with lubricating oil at the initial moment of the simulation. Although the baffle structure can hinder the leakage of the lubricating oil from the oil inlet hole to the sealing gap, it also hinders the flow of the lubricating oil between the baffle and the sealing gap. Therefore, the lubricating oil that should have flowed out through the oil return port can only leak through the sealing gap. As a result, the leakage of the lubricating oil increases with the increase in the baffle height, which is the accumulation effect of the lubricating oil caused by the baffle. The oil leakage of the structure with a baffle height of 10 mm was greater than that of the structure with a baffle height of 5 mm before 2.5 s due to the

accumulation effect, but it was less than 5 mm after 2.5 s due to the baffle blocking the oil from the inlet to the sealing gap. The leakage is basically between 0 and 30 g/s.

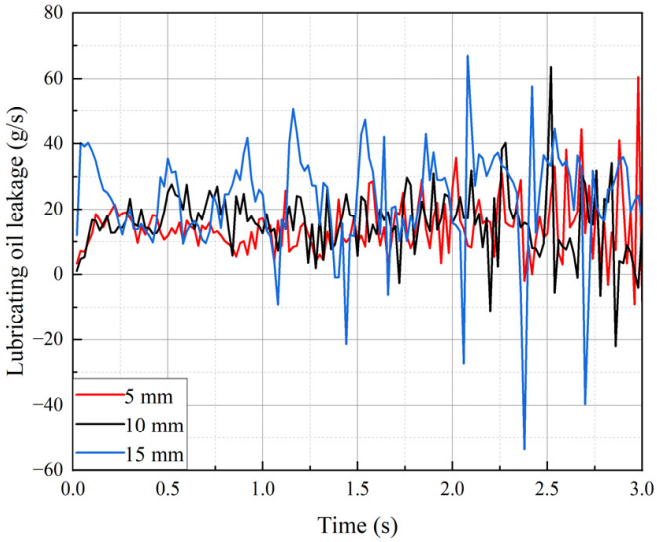


Figure 16. Variation in oil leakage with different baffle heights (ΔP = 7.5 kPa, n = 15,000 r/min).

4.1.2. The Sealing Pressure Difference Is 10 kPa and the Rotational Speed Is 15,000 r/min

Figure 17 shows the variation in oil leakage with different baffle heights under the condition of a sealing pressure difference of 10 kPa and rotating speed of 15,000 r/min. It can be seen that the higher the height of the baffle, the greater the amount of oil leakage. The leakage in Figure 17 is generally smaller than that in Figure 16 with the same structural parameters. When the sealing pressure difference is 10 kPa, the leakage of the baffle height of 15 mm is basically within 40 g/s, and the leakage of the baffle height of 5 mm is basically within 20 g/s. At the initial time, due to the existence of lubricating oil between the baffle structure and the graphite sealing gap, the leakage of lubricating oil will surge to a higher value. The structure with a baffle height of 15 mm has a higher baffle height, so the leakage before 0.25 s is much higher than the other two: close to 40 g/s. The oil leakage and variation law of the baffle height of 5 mm and 10 mm are close, indicating that the sealing effect of the two baffle heights is close under this working condition, which may be due to the better sealing effect when the sealing pressure difference is 10 kPa.

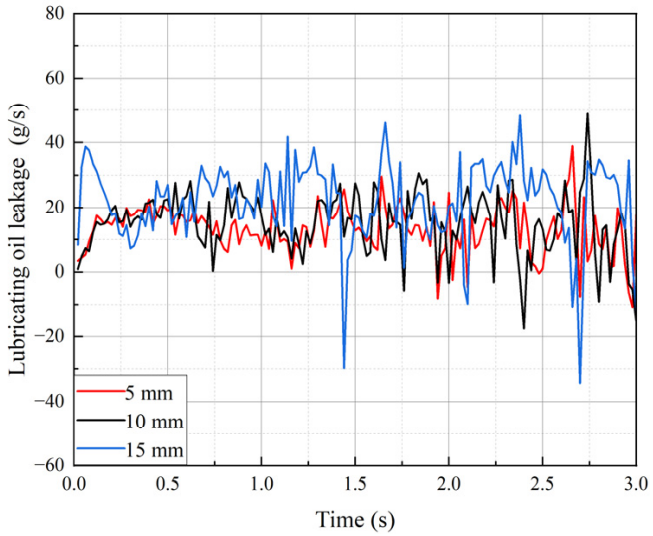


Figure 17. Variation in oil leakage with different baffle heights (ΔP = 10 kPa, n = 15,000 r/min).

4.1.3. The Sealing Pressure Difference Is 7.5 kPa and the Rotational Speed Is 10,000 r/min

Figure 18 shows the change in oil leakage with different baffle heights under the condition of a sealing pressure difference of 7.5 kPa and rotational speed of 10,000 r/min. It can be seen that with the increase in baffle height, the leakage of lubricating oil also increases. When the baffle height is 15 mm, the oil leakage fluctuates in the range of 0–20 g/s, exceeding this range at some moments, and the oil leakage is greater than the other two baffle heights. In Figure 18, the difference of oil leakage under three different baffle heights is not large. This is because the centrifugal force of oil is small due to the low speed, and the influence of oil accumulation is weakened, so that the change in oil leakage is small. When the baffle height is 10 mm, the oil leakage is slightly higher than that of the baffle height of 5 mm, but the peak value is higher than the other two baffle heights. When the baffle height is 5 mm, the oil leakage is the smallest and fluctuates in the range of 0~20 g/s.

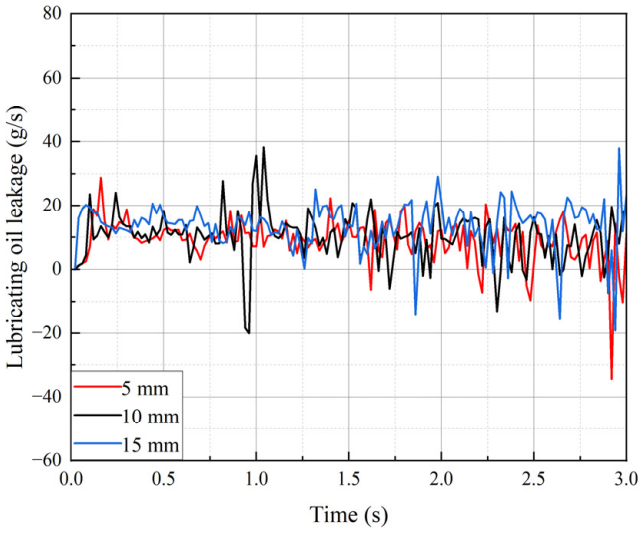


Figure 18. Variation in oil leakage with different baffle heights (ΔP = 7.5 kPa, n = 10,000 r/min).

4.2. The Influence of Sealing Pressure Difference on the Bearing Chamber Sealing System with Baffle

4.2.1. The Baffle Height Is 15 mm and the Rotational Speed Is 15,000 r/min

Figure 19 shows the change in oil leakage with different sealing pressure differences under the condition of a baffle height of 15 mm and rotational speed of 15,000 r/min. It can be seen that with the increase in sealing pressure difference, the oil leakage decreases slightly. At the initial time, due to the high speed, large centrifugal effect and large accumulation of lubricating oil, the leakage surge occurs. When the sealing pressure difference is 7.5 kPa, the oil leakage is significantly greater than the other two sealing pressure differences, and the peak value is close to 70 g/s. When the sealing pressure difference is 15 kPa, the oil leakage fluctuates in the range of 0~40 g/s. The degree of fluctuation decreases with the increase in sealing pressure difference. This is because the larger the sealing pressure difference, the more sufficient the gas volume, which can better inhibit the leakage of lubricating oil.

4.2.2. The Baffle Height Is 10 mm and the Rotational Speed Is 15,000 r/min

Figure 20 shows the change in oil leakage with different sealing pressure differences under the condition of a baffle height of 10 mm and rotating speed of 15,000 r/min. It can be seen that with the increase in sealing pressure difference, the oil leakage decreases slightly. Compared with Figure 19, the height of the baffle is reduced, the average oil leakage is reduced, and the degree of fluctuation is reduced, which is consistent with the

analysis results in the previous section. Before 2.5 s, due to the low leakage of lubricating oil, the leakage channel formed at the graphite sealing gap is large, so the response degree to the change in sealing pressure difference is low, and the leakage of the different sealing pressure differences is similar. The leakage of lubricating oil fluctuates within 0–35 g/s. After 2.5 s, the fluctuation degree of oil leakage decreases with the increase in sealing pressure difference due to the decrease in accumulation effect.

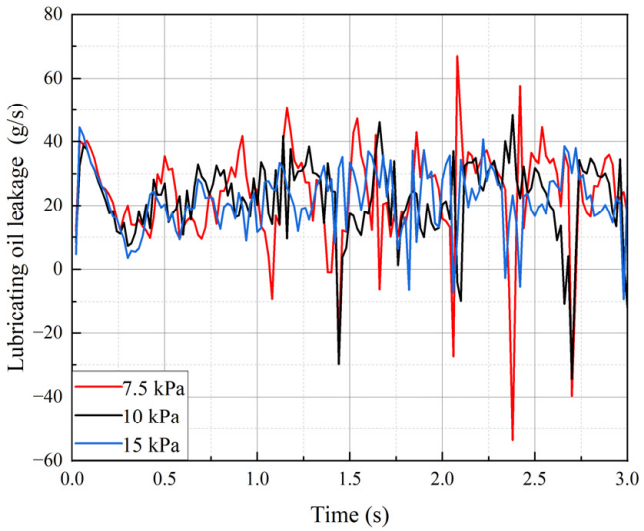


Figure 19. Variation in oil leakage with different sealing pressure difference (h = 15 mm, n = 15,000 r/min).

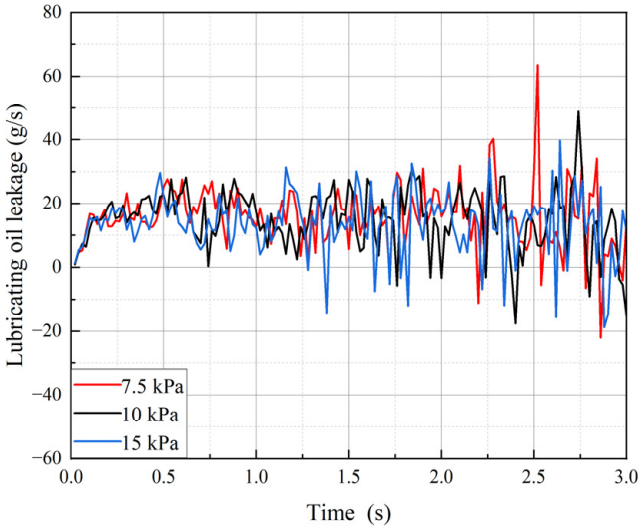


Figure 20. Variation in oil leakage with different sealing pressure difference (h = 10 mm, n = 15,000 r/min).

4.2.3. The Baffle Height Is 15 mm and the Rotational Speed Is 5000 r/min

Figure 21 shows the change in oil leakage with different sealing pressure differences under the condition of a baffle height of 15 mm and rotational speed of 5000 r/min. It can be seen that with the increase in sealing pressure difference, the oil leakage decreases slightly and the fluctuation degree decreases. Due to the low rotational speed, the centrifugal effect of lubricating oil is low, and the kinetic energy is low, which is not enough to cross the graphite sealing gap and make the leakage of lubricating oil low. The average leakage of lubricating oil under different sealing pressure differences is not more than 3 g/s, and the peak value is not more than 5 g/s. It is worth noting that when the height of the baffle is 15 mm, the sealing pressure difference is 15 kPa, and the rotational speed is 5000 r/min. Except for the surge of oil leakage due to the accumulation effect at the beginning, the oil

leakage at the rest of the time is close to 0 g/s or negative, indicating that the critical sealing state has been reached or exceeded under this working condition—that is, the oil just does not leak. Under this working condition, the graphite sealing system of the bearing chamber with the baffle configuration has good sealing characteristics.

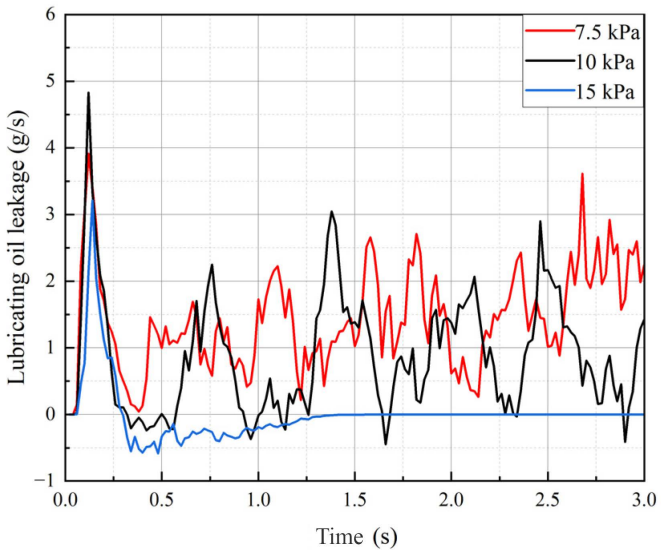


Figure 21. Variation in oil leakage with different sealing pressure difference (h = 15 mm, n = 5000 r/min).

4.3. The Influence of Rotational Speed on the Bearing Chamber Sealing System with Baffle Configuration

4.3.1. The Baffle Height Is 15 mm and the Sealing Pressure Difference Is 10 kPa

Figure 22 shows the variation in oil leakage with different rotational speeds under the condition of a baffle height of 15 mm and sealing pressure difference of 10 kPa. It can be seen from the diagram that with the substantial increase in the rotational speed, the amount of oil leakage has also increased significantly. The oil leakage at 15,000 r/min is significantly greater than that at 10,000 r/min and 5000 r/min, but it is basically kept within 40 g/s. When the rotational speed is 10,000 r/min, the oil leakage of the bearing chamber is basically within 0~30 g/s, and the fluctuation is less than that when the rotational speed is 15,000 r/min. This is due to the large increase in the rotational speed. The degree of turbulence in the chamber increases and the degree of fluctuation increases. When the speed is 5000 r/min, the oil leakage is much smaller than the other two speeds, and it fluctuates in the range of 0~3 g/s. This is because the sealing pressure difference is large, the speed is low, and the sealing effect is better. The red curve in Figure 22 and the black curve in Figure 21 show the same working condition.

4.3.2. The Baffle Height Is 10 mm and the Sealing Pressure Difference Is 10 kPa

Figure 23 shows the variation in oil leakage with different rotational speeds under the condition of a baffle height of 10 mm and a sealing pressure difference of 10 kPa. It can be seen from the diagram that the higher the rotational speed, the greater the oil leakage. When the speed is 15,000 r/min, the oil leakage is in the range of 0~30 g/s, the peak value is 50 g/s, and the oil leakage is higher than the other two speeds. When the speed is 10,000 r/min, the oil leakage is in the range of 0~20 g/s, some times more than 20 g/s, and the peak reaches 60 g/s. When the speed is 5000 r/min, the oil leakage is the smallest. This is because with the rapid increase in the rotational speed, the shear effect of the rotating shaft on the oil, gas and oil–gas mixture in the bearing chamber is greatly enhanced, and the turbulence in the bearing chamber is enhanced, so that the oil has greater kinetic energy to leak through the graphite sealing gap to the sealing chamber.

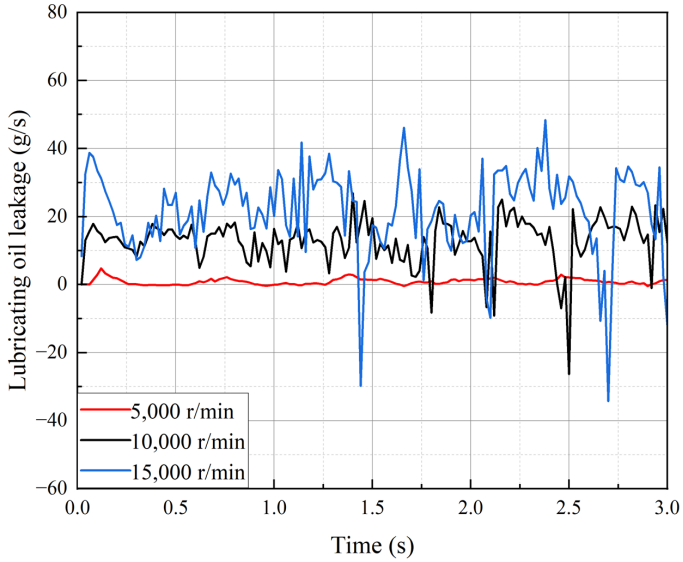


Figure 22. Variation in oil leakage with different rotational speed (h = 15 mm, ΔP = 10 kPa).

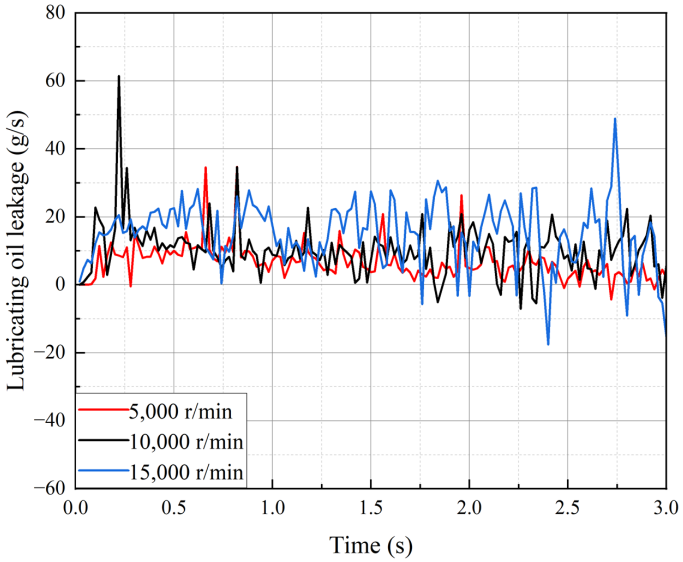


Figure 23. Variation in oil leakage with different rotational speed (h = 10 mm, ΔP = 10 kPa).

4.3.3. The Baffle Height Is 15 mm and the Sealing Pressure Difference Is 7.5 kPa

Figure 24 is the change in oil leakage with different rotational speeds under the condition of a baffle height of 15 mm and sealing pressure difference of 7.5 kPa. It can be seen that the oil leakage increases with the increase in rotational speed. Compared with Figure 22, the sealing pressure difference is reduced. Compared with the oil leakage at the same speed, it is found that the oil leakage increases slightly and the fluctuation degree increases with the decrease in the sealing pressure difference, which is consistent with the conclusion of the previous section. When the speed is 15,000 r/min, the oil leakage is in the range of 0~40 g/s, and some of the time exceeds this range; the peak value is close to 70 g/s. The average oil leakage is much higher than the oil leakage when the speed is 10,000 r/min and 5000 r/min. This is due to the increase in the centrifugal effect of the oil caused by the large increase in the speed, which increases the leakage capacity of the oil. When the rotational speed is 10,000 r/min, the oil leakage is mostly in the range of 0~20 g/s. When the rotational speed is 5000 r/min, the oil leakage is mostly in the range of 0~5 g/s. With the increase in rotational speed, the oil leakage also increases.

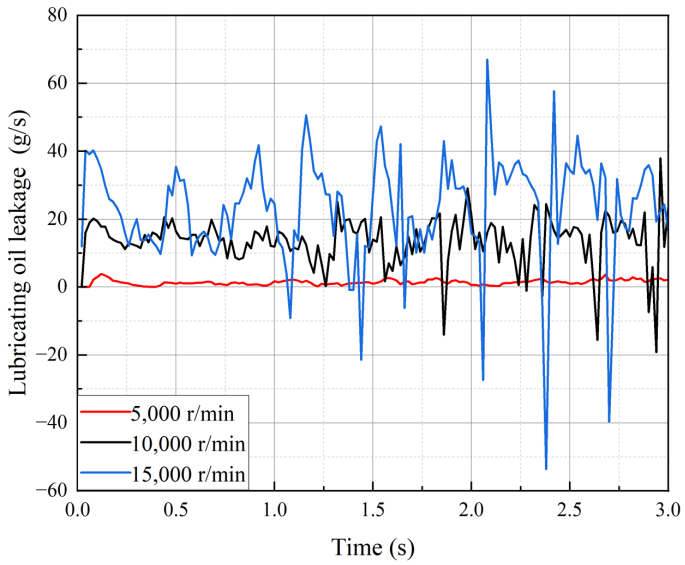


Figure 24. Variation in oil leakage with different rotational speed (h = 15 mm, ΔP = 7.5 kPa).

4.4. Summary of This Section

This section analyzes the influence of baffle height, sealing pressure difference and rotational speed on the oil leakage of bearing chamber sealing system with a baffle configuration, and it draws the following conclusions:

(1) Due to the accumulation effect of the lubricating oil after adding the baffle, the higher the baffle height, the more serious the accumulation, so the leakage of the lubricating oil increases with the increase in the baffle height.

(2) With the increase in sealing pressure difference, the leakage of the lubricating oil decreases slightly, and the fluctuation of leakage of the lubricating oil decreases.

(3) The increase in rotational speed increases the centrifugal effect of the lubricating oil, which makes it easier for the lubricating oil to cross the sealing gap and leak. Therefore, the leakage of the lubricating oil increases with the increase in rotational speed.

(4) At the same rotational speed, after increasing the sealing pressure difference, the average oil leakage of the bearing chamber sealing systems with different baffle heights decreases and the fluctuation degree decreases; at the same rotational speed, upon reducing the height of the baffle, the average oil leakage of the bearing chamber sealing system with different sealing pressure differences is reduced; under the same sealing pressure difference, the average oil leakage of the bearing chamber sealing systems with different baffle heights decreases with the decrease in rotational speed; under the same sealing pressure difference, after reducing the height of the baffle, the average oil leakage of the bearing chamber sealing system at different rotational speeds is reduced; under the same baffle height, upon reducing the sealing pressure difference, the average oil leakage of the bearing chamber sealing system at different rotational speeds increases; at the same baffle height, the average oil leakage of the bearing chamber sealing system with different sealing pressure difference decreases with the decrease in rotational speed.

Therefore, for the bearing chamber sealing system with a baffle configuration, the height of the baffle can be appropriately reduced, the sealing pressure difference can be increased, and the rotational speed can be reduced to reduce the oil leakage.

Author Contributions: Writing—review and editing, G.R.; writing—original draft preparation, R.W.; resources, M.W.; project administration, H.Z.; supervision, W.X. All authors have read and agreed to the published version of the manuscript.

Funding: This research received no external funding.

Data Availability Statement: The original contributions presented in this study are included in the article. Further inquiries can be directed to the corresponding author.

Acknowledgments: The authors are grateful to the reviewers for their careful and detailed comments.

Conflicts of Interest: Author Mingzhang Wang was employed by the company Aero Engine Corporation of China (AECC). The remaining authors declare that the research was conducted in the absence of any commercial or financial relationships that could be construed as a potential conflict of interest.

References

1. Guo, J.; Zhao, H.; Wang, P.; Sun, D.; Wang, S. Numerical and experimental study on oil-air two-phase, leakage flow characteristics based on air-bleeding oil-sealing mode in seal clearance of bearing cavity. *J. Mech. Eng.* **2024**, *3*, 214–225. [CrossRef]
2. Wang, L.N.; Chen, G.D.; Sun, H.C. Characteristics analysis of oil droplet deposition and oil film in a bearing chamber. *Acta Aeronaut. Astronaut. Sin.* **2016**, *37*, 3159–3169. [CrossRef]
3. Sun, H.C.; Chen, G.D.; Wang, L.N.; Wang, F. Oil droplets fractions and oil droplets/air energy transfer analysis in bearing chamber. *Acta Aeronaut. Astronaut. Sin.* **2016**, *37*, 1060–1073. [CrossRef]
4. Wang, L.; Chen, G.; Sun, H. Deposition characteristic of the oil droplet on housing in a bearing chamber. *J. Harbin Inst. Technol.* **2017**, *49*, 144–149. [CrossRef]
5. Fang, L.; Chen, G. The Experimental and Theoretical Study of Oil Droplet Behaviors after Oblique Collision in Bearing Chamber. *J. Northwestern Polytech. Univ.* **2016**, *34*, 627–634.
6. Li, K.; Gao, W.; Li, W.; Zhang, J.; Li, C.; Liu, Z. Numerical Study of Oil-Air Two-Phase Flow and Heat Transfer in Tapered Bearing Chamber. *J. Propuls. Technol.* **2022**, *43*, 251–259. [CrossRef]
7. Li, W. Numerical Simulation and Research on the Characteristics of Oil/Gas Two-Phase Flow in Bearing Chamber. Master's Thesis, Nanjing University of Aeronautics and Astronautics, Nanjing, China, 2017.
8. Ren, G.; Yan, Y.; Zheng, G.; Zhao, H.; Sun, D.; Zhang, C. Oil-Gas Two-Phase Flow Characteristics and Improvement of Bearing Chamber for an Aeroengine. *J. Propuls. Technol.* **2023**, *44*, 165–174. [CrossRef]
9. Hu, J.P.; Ren, G.Z.; Yi, J.; Liu, Z.X.; Lu, Y.G.; Zhao, J.Y. Numerical simulation and experiment for heat transfer between oil film and inner wall of bearing chamber. *Acta Aeronaut. Astronaut. Sin.* **2017**, *38*, 521013. [CrossRef]
10. Ren, G. Study on Flow and Heat Transfer and Optimization of Scavenge Structure in Bearing Chamber Based on Oil/Air Two-Phase Flow. Ph.D. Thesis, Northwestern Polytechnical University, Xi'an, China, 2016.
11. Cao, Y.T.; Lyu, Y.G.; Zhu, Z.T.; Li, W.R.; Liu, Z.X. Numerical study of two-phase flow and heat transfer characteristics of double fulcrum counter-rotating bearing chamber. *J. Propuls. Technol.* **2024**, *45*, 2305038. [CrossRef]
12. Cao, Y.; Zhong, Y.; Wu, Y.; Zhou, L.; Su, Z. Influence of sealing air mass flow rate on bearing chamber outer wall oil movement. *Aeroengine* **2023**, *49*, 127–133. [CrossRef]
13. Gu, J. Study on Oil Scavenge Characteristics of Aero-Engine Bearing Chamber. Master's Thesis, Jiangsu University, Zhenjiang, China, 2023.
14. Li, C. Research on Transfercharacteristics of Oil/Gas Two-Phase in a Ventless Aero-Engine Bearing Chamber. Master's Thesis, Shenyang Aerospace University, Shenyang, China, 2022.
15. Li, Y.; Yang, F.; Liu, Z.X.; Zhang, C.Y.; Lu, Y.G. Flow and thermal analysis of oil air two-phase medium in bearing chamber. *J. Aerosp. Power* **2021**, *36*, 606–615. [CrossRef]
16. Wang, B.; Bai, C.; Wang, Z. Effect of oil-air outlet location on oil-air two-phase flow and temperature rise in bearing cavity. *Lubr. Eng.* **2020**, *45*, 28–33. [CrossRef]
17. Yang, P.; Lu, P.; Fang, L.; Wang, X. Effects of structure parameters of scavenge sump on oil/air two-phase flow in bearing chamber. *J. Jiangsu Univ. (Nat. Sci. Ed.)* **2019**, *40*, 643–648. [CrossRef]
18. Yang, P. Study on the Flow Pattern and Oil Scavenge Characteristics in an Aero-Engine Bearing Chamber. Master's Thesis, Nanjing University of Aeronautics and Astronautics, Nanjing, China, 2019.
19. Fang, L. Study on the Oil-Gas Two-Phase Flow and Heat Transfer in an Aero-Engine Bearing Chamber and the Scavenge Pipes. Master's Thesis, Nanjing University of Aeronautics and Astronautics, Nanjing, China, 2020.
20. Lv, Y.; Zhang, M.; Liu, Z.; Hu, J. Numerical study and validation for two-phase flow of oil and gas in aero-engine bearing cavity. *J. Aerosp. Power* **2014**, *29*, 2751–2757. [CrossRef]
21. Hu, Z. Research on Two-Phase Flow Characteristics of Oil-Gas in Aero-Engine Bearing Chamber. Master's Thesis, Shenyang Aerospace University, Shenyang, China, 2021.
22. Glahn, A.; Busam, S.; Blair, M.F.; Allard, K.L.; Wittig, S. Droplet Generation by Disintegration of Oil Films at the Rim of a Rotating Disk. *J. Eng. Gas Turbines Power* **2002**, *124*, 117–124. [CrossRef]

23. Glahn, A.; Blair, M.F.; Allard, K.L.; Busam, S.; Schafer, O.; Wittig, S. Disintegration of Oil Jets Emerging From Axial Passages at the Face of a Rotating Cylinder. *J. Eng. Gas Turbines Power* **2003**, *125*, 1003–1010. [CrossRef]
24. Glahn, A.; Blair, M.F.; Allard, K.L.; Busam, S.; Schafer, O.; Wittig, S. Disintegration of Oil Films Emerging From Radial Holes in a Rotating Cylinder. *J. Eng. Gas Turbines Power* **2003**, *125*, 1011–1020. [CrossRef]
25. Lee, C.W.; Palma, P.C.; Simmons, K.; Pickering, S.J. Comparison of Computational Fluid Dynamics and Particle Image Velocimetry Data for the Airflow in an Aeroengine Bearing Chamber. *ASME J. Eng. Gas Turbines Power* **2005**, *127*, 697–703. [CrossRef]
26. Gorse, P.; Willenborg, K.; Busam, S.; Ebner, J.; Dullenkopf, K.; Wittig, S. 3D-LDA Measurements in an Aero-Engine Bearing Chamber. In Proceedings of the ASME Turbo Expo 2003, Collocated with the 2003 International Joint Power Generation Conference, Atlanta, GA, USA, 16–19 June 2003. [CrossRef]
27. Aidarinis, J.; Missirlis, D.; Yakinthos, K.; Goulas, A. CFD Modelling and LDA Measurements for the Air-Flow in an Aero-Engine Front Bearing Chamber. In Proceedings of the ASME Turbo Expo 2010: Power for Land, Sea, and Air, Glasgow, UK, 14–18 June 2010; pp. 1201–1208. [CrossRef]
28. Farrall, M.; Simmons, K.; Hibberd, S.; Gorse, P. A Numerical Model For Oil Film Flow in an aero-engine Bearing Chamber and Comparison with Experimental data. In Proceedings of the ASME Turbo Expo: Power for Land, Sea, and Air, Vienna, Austria, 14–17 June 2004; pp. 409–417. [CrossRef]
29. Chew, J.W. Analysis of the Oil Film on the Inside Surface of an Aero-Engine Bearing Chamber Housing. In Proceedings of the ASME 1996 International Gas Turbine and Aeroengine Congress and Exhibition, Birmingham, UK, 10–13 June 1996. [CrossRef]
30. Farrall, M.B.; Hibberd, S.; Simmons, K. Computational modelling of two-phase air/oil flow within an aero-engine bearing chamber. *Int. J. Comput. Fluid Dyn.* **2000**, *7*, 318–328.
31. Hashmi, A.A.; Dullenkopf, K.; Koch, R.; Bauer, H.J.R. CFD Methods for Shear Driven Liquid Wall Films. In Proceedings of the ASME Turbo Expo 2010: Power for Land, Sea, and Air, Glasgow, UK, 14–18 June 2010; Volume 4, pp. 1283–1291. [CrossRef]
32. Peduto, D.; Hashmi, A.A.; Dullenkopf, K.; Bauer, H.J.R.; Morvan, H. Modelling of an Aero-Engine Bearing Chamber Using Enhanced CFD Technique. In Proceedings of the ASME 2011 Turbo Expo: Turbine Technical Conference and Exposition, Vancouver, BC, Canada, 6–10 June 2011; Volume 5, pp. 809–819. [CrossRef]
33. Crouchez, P.A.; Morvan, H.P. CFD Simulation of an Aeroengine Bearing Chamber Using an Enhanced Volume of Fluid (VOF) Method: An Evaluation Using Adaptive Meshing. In Proceedings of the ASME Turbo Expo 2014: Turbine Technical Conference and Exposition, Düsseldorf, Germany, 16–20 June 2014; Volume 5C. [CrossRef]
34. Adeniyi, A.A.; Morvan, H.P.; Simmons, K.A. A Transient CFD Simulation of the Flow in a Test Rig of an Aeroengine Bearing Chamber. In Proceedings of the ASME Turbo Expo 2014: Turbine Technical Conference and Exposition, Düsseldorf, Germany, 16–20 June 2014; Volume 5C. [CrossRef]
35. Wieth, L.; Lieber, C.; Kurz, W.; Braun, S.; Koch, R.; Bauer, H.J. Numerical Modeling of an Aero-Engine Bearing Chamber Using the Meshless Smoothed Particle Hydrodynamics Method. In Proceedings of the ASME Turbo Expo 2015: Turbine Technical Conference and Exposition, Montreal, QC, Canada, 15–19 June 2015; Volume 2B. [CrossRef]
36. Ren, G.; Li, Y.; Zhao, H.; Xu, W.; Sun, D.; Yan, Y. Research on flow characteristics of bearing chamber sealing system based on oil-gas two-phase flow. *J. Aerosp. Power* **2025**, *40*, 285–296. [CrossRef]

Disclaimer/Publisher's Note: The statements, opinions and data contained in all publications are solely those of the individual author(s) and contributor(s) and not of MDPI and/or the editor(s). MDPI and/or the editor(s) disclaim responsibility for any injury to people or property resulting from any ideas, methods, instructions or products referred to in the content.